Optimizing safety and comfort for distracted drivers via adaptive shared control

Lyuchao Liao, Pengqi Xing* [iD], Zhenhua Gan, Xiaohui Wei and Yan Liu

School of Transportation, Fujian University of Technology, No. 69, Xue fu nan Road, Shang jie Town, Fuzhou 350118, China
* Corresponding author, E-mail: pengqi@smail.fjut.edu.cn

Abstract

Driver distraction introduces considerable uncertainty in vehicle operation, presenting significant challenges to driving safety and complicating human-machine collaborative control. To address these challenges, this paper proposes a shared control approach to support distracted drivers in maneuvering along extended curves. A model of distracted driver behavior is first constructed to simulate both path-following capability and distraction duration, capturing the operational characteristics of distracted drivers. Building upon this model, a multi-constraint model predictive controller (H-ORPF-MPC) is developed, integrating driver behavior and environmental factors to balance driving comfort and controller stability. Surrounding risks are quantified through a driver intention function and an Obstacle-Road Potential Field (ORPF), with real-time state constraint envelopes applied to control outputs, thereby ensuring vehicle operation within a safe range. Furthermore, safety and comfort-based authority allocation rules are formulated, accommodating both controller performance and driver preferences. Simulation results indicate that the proposed approach effectively assists distracted drivers, significantly reduces trajectory tracking errors, and improves driving comfort.

Keywords: Human-machine cooperative control; Distracted driver behavior; Muti-constraints MPC; Driver operating characteristics

Introduction

With the increasing availability of in-vehicle entertainment functions, driver distraction has emerged as a critical safety issue. Even seemingly minor tasks, such as adjusting temperature controls or using navigation systems, can significantly impair a driver's focus on the road[1]. Driver distraction can lead to operational errors, severely compromising safety. Investigations into traffic accidents consistently highlight driver inattention as a primary factor in severe injury accidents. For instance, a study analyzing 340 cases found that 57.6% of drivers were inattentive, with an additional 5.9% potentially inattentive. Née et al.[2] examined the role of driver distraction in road traffic accidents, surveying 1,912 drivers involved in such incidents. The study identified activities that diverted the driver's attention away from the road or caused them to remove their hands from the steering wheel as significant contributors to accident responsibility. These findings underscore the necessity for driver assistance systems that can enhance vehicle performance when drivers are distracted.

Recent advancements in artificial intelligence have led to significant progress in autonomous driving technologies. Nevertheless, due to societal concerns regarding acceptance, privacy issues[3], precise network transmission challenges[4], and the complexity of navigating intricate road networks, human drivers are expected to remain integral participants or even primary operators for the foreseeable future. Until fully autonomous driving becomes a reality, human-machine co-driving, where control is shared between drivers and automated systems, has gained widespread acceptance. This approach enables drivers to leverage autonomous driving systems while retaining control, effectively correcting inappropriate human driving behaviors[5].

In shared human-machine co-driving systems, both the driver and the automated system contribute to vehicle control, interacting dynamically through control mechanisms that allow real-time adjustments. This interaction enables the system to harness the driver's operational characteristics, thereby improving overall vehicle control performance. Within this framework, the driver's behavior plays a pivotal role, significantly influencing the effectiveness of collaborative control.

Current research on driver behavior and shared control systems emphasizes the critical importance of understanding driver behavior to improve road safety and advance the development of autonomous vehicles[6]. Studies conducted both domestically and internationally demonstrate that incorporating driver behavior into controller design can enhance traffic efficiency and increase the effectiveness of driver assistance systems. Domestically, researchers have conducted in-depth studies on driver behavior modeling, managing uncertainties in driving behavior and improving controller robustness. For instance, Jiang et al.[7], developed an adaptive steering feedback torque system by analyzing drivers' compensation mechanisms in response to changes in steering feedback. Another study[8] improved system robustness by introducing random perturbations and various traffic scenarios to simulate behavioral uncertainties among different drivers. Jiang et al.[9] integrated driver uncertainties and vehicle dynamics into trajectory prediction, achieving more accurate long-term predictions. Similarly, Chen et al.[10] proposed a robust driver assistance controller that enhanced collaboration between human drivers and automated controllers during switching scenarios by accounting for uncertainties in driver model parameters. Inspired by professional driver behavior, Chen et al.[11] designed a robust steering controller capable of achieving precise control under model uncertainties and external disturbances. Internationally, significant progress has been made in improving interactions between human drivers and control systems while enhancing system robustness to uncertainties and

dynamic changes. Nguyen et al.[12] applied the Takagi-Sugeno fuzzy control method to incorporate driver behavior into the control loop, dynamically adjusting time-varying driver activity parameters and vehicle speed to improve safety and comfort. Sentouh et al.[13] developed a driver model combining visual prediction and compensation, suitable for both novice and experienced drivers and designed an H∞ robust controller within a dual -loop human-machine shared control structure to minimize vehicle trajectory tracking errors. Chen et al.[14] addressed the risks posed by impaired drivers by proposing an impaired steering behavior model and developing a Gain-Scheduling Compound Nonlinear Feedback (GCNF) controller to assist steering, reducing steering angle deviations and driver workload. Additionally, Singh et al.[15] employed a Weighted Online Extended Dynamic Mode Decomposition (WOEDMD) algorithm to update driver models in real-time during obstacle avoidance, thereby improving driving safety.

These studies collectively highlight the importance of incorporating driver behavior into the design of vehicle control systems. However, a significant gap remains in addressing the dynamic state of drivers, particularly in scenarios involving distraction. Most existing research focuses on enhancing vehicle control performance through advanced control algorithms, often modeling drivers and designing controllers independently. This approach tends to overlook the impact of driver behavior on controller stability and fails to consider drivers' subjective comfort. Furthermore, road conditions such as curves and intersections can amplify the risks associated with driver distraction[16]. An analysis of crash data from 15 US states between 2013 and 2017 found that certain built environments, including curves, intersections, and work zones, significantly increase the likelihood of injuries in accidents involving distracted driving. Despite these findings, few studies have specifically targeted the development of driver assistance controllers for distracted drivers in long curve scenarios.

Research on driving authority allocation between humans and machines generally falls into two categories. The first adjusts driving authority based on the driver's state or intention. For example, the study by Huang et al.[17] detects driver steering intention through geometric relationships and intervenes when steering behavior is deemed inappropriate. Flad et al.[18] used a semi-supervised learning algorithm to predict lane-changing intentions based on steering wheel angles and pedal inputs, thereby improving vehicle stability during lane changes. Another study by Fang et al.[19] employed a Gaussian-Bernoulli Restricted Boltzmann Machine to assess driving intentions and adjust driving authority in real-time. Sentouh et al.[13] used a Driver Monitoring System (DMS) to assess driver states, facilitating smooth transitions between driver and Lane Keeping Assist (LKA) control. Li et al.[20] developed a perception function to better represent drivers' sensitivity to distance, using experimental data to model real-world reaction times and enhance collaboration between human drivers and automated systems.

The second category of research focuses on adjusting driving authority based on assessed driving risks. For instance, Jiang et al.[21] proposed a two-layer sequence prediction algorithm using Long Short-Term Memory (LSTM) to detect lane-changing intentions and design a safety-oriented decision-making mechanism. In the study by Dong et al.[22], a fuzzy controller was employed to infer control weight distribution coefficients, creating a model that adjusts driving authority in real time based on vehicle distance and longitudinal motion risks. Zhao et al.[23] developed a Gaussian Process Regression (GPR) model to evaluate cornering risks, generating safety envelopes to allocate control authority between drivers and machines.

However, solely considering driver intention or driving risk in authority allocation can result in control strategies that either overemphasize comfort at the expense of safety or focus excessively on safety, potentially diminishing the driving experience. A balanced approach that integrates both driver intention and driving risk is essential for ensuring optimal safety and comfort. This work introduces a shared control strategy that accounts for the behavior of distracted drivers. The contributions of this study are summarized as follows:

(1) A model predictive controller considering driver behavior and the obstacle-road potential field (H-ORPF-MPC) is developed that integrates driver behavior and environmental conditions to balance driving comfort with controller stability. The proposed controller uses a driver intention function and an obstacle-road potential field (ORPF) to quantify risks from surrounding obstacles and road boundaries. A state constraint envelope is employed to ensure real-time safe operation of the vehicle.

(2) A balanced authority allocation mechanism is proposed that considers both road safety and driver subjective comfort, enhancing the effectiveness of driver assistance. Three functions were designed to evaluate the road environment and driver distraction levels. Lateral risk in the road environment combines road width and vehicle deviation; longitudinal risk utilizes *TTC* with the *TTCi* formula; and driver distraction level is assessed based on the difference between the driver's steering output and the desired steering angle. Fuzzy rules were designed based on the driver's state while considering vehicle safety, and a fuzzy controller was used to calculate the cooperation factor.

(3) A distracted driver model was constructed to capture path-following ability and distraction duration. Using a single-point preview driver model based on sliding mode control as the baseline, the model introduced reaction delay and correction components to simulate the delayed reaction characteristics of distracted drivers. During modeling, driver steering input and parameter uncertainties were considered, and real vehicle test data were incorporated to model the delayed reaction characteristics of distracted drivers.

System modeling for driver-integrated control

In this section, the vehicle dynamics model and distracted driver model are established to facilitate the shared controller design in the next section. The distracted driver model will imitate the human driver to control the vehicle, and the vehicle dynamics model will serve as the basic part of the multi-constraint MPC in the next section. Finally, a simulation test was conducted on the distracted driver model.

Vehicle dynamics model

The single-track model of a vehicle is illustrated in Fig. 1. Here, (*X*, *Y*) represents the coordinates of the vehicle's center of gravity in the global coordinate system, and (*x*, *y*) represents the vehicle coordinate system. Considering the lateral, longitudinal, and yaw movements of the vehicle, the vehicle dynamics model can be derived using Newton's second law[24–25]:

$$\begin{cases} ma_y = F_{yf} + F_{yr} \\ ma_x = F_d - F_{xf} \\ I_z\ddot{\varphi} = l_aF_{cf} - l_bF_{cr} \end{cases} \quad (1)$$

The parameter m represents the vehicle's mass, while F_{cf} and F_{cr} represent the lateral forces acting on the front and rear wheels, respectively. F_{yf} and F_{yr} correspond to the lateral forces on the front and rear wheels, respectively, while F_{xf} denotes the longitudinal force on the front wheels. I_z represents the moment of inertia of the vehicle about the z-axis, and φ denotes the yaw angle. The distances
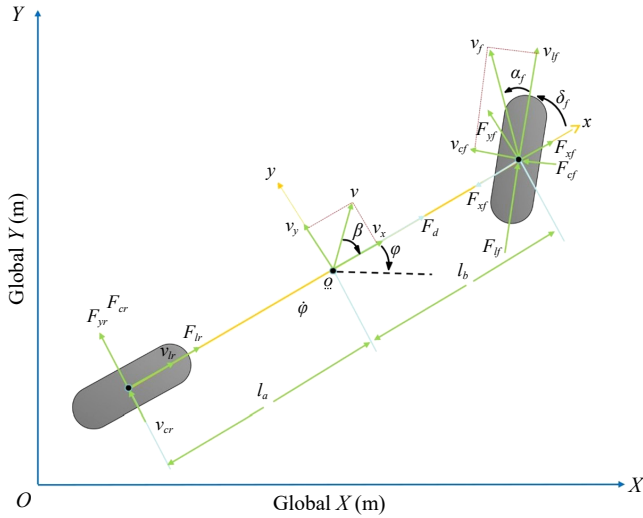
Adaptive shared control for distracted drivers

Fig. 1 Vehicle dynamics model.

l_a and l_b measure the distance from the center of mass to the front and rear axles, respectively. a_x and a_y are the longitudinal and lateral inertial accelerations of the vehicle at the center of mass o.

$$\begin{cases} a_y = \ddot{y} + v_x\dot{\varphi} \\ a_x = \dot{v}_x - v_y\dot{\varphi} \end{cases} \tag{2}$$

From the geometric relationships in the figure:

$$\begin{cases} F_{xf} = F_{cf}sin\delta_f \\ F_{yf} = F_{cf}cos\delta_f \\ F_{yr} = F_{cr} \end{cases} \tag{3}$$

When the slip ratio is small, the relationship between slip ratio and lateral force is linear. The same applies to longitudinal force. Therefore, when the sideslip angle and slip ratio are small, the tire forces can be linearized to simplify the model. The tire force equations are as follows:

$$\begin{cases} F_{lf} = C_{lf}s_f \\ F_{cf} = C_{cf}\alpha_f \\ F_{lr} = C_{lr}s_r \\ F_{cr} = C_{cr}\alpha_r \end{cases} \tag{4}$$

where, C_{cf}, C_{lf} and C_{cr}, C_{lr} are the lateral stiffness of the front and rear tires, α_f and α_r are the front and rear tire sideslip angles, and s_f and s_r are the slip ratios of the front and rear tires. Based on geometric relationships in Fig. 1, we can express α_f and α_r as:

$$\begin{cases} \alpha_f = \tan^{-1}\dfrac{v_{cf}}{v_{lf}} = \delta_f - arctan\dfrac{\dot{y}+l_a\dot{\varphi}}{v_x} \\ \alpha_r = \tan^{-1}\dfrac{v_{cr}}{v_{lr}} = arctan\dfrac{l_b\dot{\varphi}-\dot{y}}{x} \end{cases} \tag{5}$$

For the global coordinates:

$$\begin{cases} \dot{X} = \dot{x}cos\varphi - \dot{y}sin\varphi \\ \dot{Y} = \dot{x}sin\varphi + \dot{y}cos\varphi \end{cases} \tag{6}$$

Combined with the above formulas, the vehicle dynamics model is obtained:

$$\begin{cases} m\ddot{x} = m\dot{y}\dot{\varphi} + 2\left[C_{lf}s_f + C_{cf}\left(\delta_f - \dfrac{\dot{y}+l_f\dot{\phi}}{\dot{x}}\right)\delta_f + C_{lr}s_r\right] \\ m\ddot{y} = -m\dot{x}\dot{\varphi} + 2\left[C_{lf}s_f\delta_f + C_{cf}\left(\dfrac{\dot{y}+l_f\dot{\varphi}}{\dot{x}} - \delta_f\right) + C_{cr}\dfrac{l_r\dot{\phi}-\dot{y}}{\dot{x}}\right] \\ I_z\dot{\varphi} = 2l_f\left[C_{lf}s_f\delta_f + C_{cf}\left(\dfrac{\dot{y}+l_f\dot{\varphi}}{\dot{x}} - \delta_f\right)\right] - 2l_rC_{cr}\dfrac{l_r\dot{\varphi}-\dot{y}}{\dot{x}} \\ \dot{X} = \dot{x}cos\varphi - \dot{y}sin\varphi \\ \dot{Y} = \dot{x}sin\varphi + \dot{y}cos\varphi \end{cases} \tag{7}$$

To facilitate subsequent controller design, this study reformulates the vehicle dynamics differential equation presented in Eq. (8) into a state-space representation form.

Take the state vector as:

$$\chi = [\dot{x}, \dot{y}, \varphi, \dot{\varphi}, X, Y]^T \tag{8}$$

The input vector is $u = \delta$. The linearized system state space equation is:

$$\dot{\chi} = A(t)\chi(t) + B(t)u(t) \tag{9}$$

$$B(t) = \begin{vmatrix} \dfrac{2C_{cf}}{m_2}\left(2\delta_f - \dfrac{\dot{y}+l_f\dot{\varphi}}{s}\right) \\ \dfrac{2\left(C_{lf}s_f - C_{cf}\right)}{m} \\ 0 \\ \dfrac{2l_f\left(C_{lf}s_f - C_{cf}\right)}{l_z} \\ 0 \\ 0 \end{vmatrix} \cdots\cdots$$

$$A(t) = \begin{bmatrix} a_{11} & a_{12} & 0 & a_{14} & 0 & 0 \\ a_{31} & a_{32} & 0 & a_{34} & 0 & 0 \\ 0 & 0 & 0 & 1 & 0 & 0 \\ a_{41} & a_{42} & 0 & a_{44} & 0 & 0 \\ a_{51} & a_{41} & a_{41} & 0 & 0 & 0 \\ a_{41} & a_{41} & a_{41} & 0 & 0 & 0 \end{bmatrix}$$

$a_{11} = \dfrac{2C_{cf}\delta_f - \left(\dot{y}+l_f\dot{\varphi}\right)}{m\dot{x}^2}$, $a_{12} = \dot{\varphi} - \dfrac{2C_{cf}\delta_f}{m\dot{x}}$, $a_{14} = \dot{y} - \dfrac{2C_{cf}l_f\delta_f}{m\dot{x}}$

$a_{21} = -\dot{\varphi} - \dfrac{2C_{cf}\left(\dot{y}+l_f\dot{\varphi}\right)+2C_{cf}\left(l_r\dot{\varphi}-\dot{y}\right)}{m\dot{x}^2}$, $a_{22} = \dfrac{2C_{cf} - 2C_{cr}}{m\dot{x}}$,

$a_{24} = -\dot{x} + \dfrac{2\left(C_{lf}l_f + C_{cf}l_r\right)}{m\dot{x}}$, $a_{41} = -\dot{\varphi} - \dfrac{2C_{cf}\left(\dot{y}+l_f\dot{\varphi}\right)+2C_{cf}\left(l_r\dot{\varphi}-\dot{y}\right)}{m\dot{x}^2}$,

$a_{42} = \dfrac{2C_{cf} - 2C_{cr}}{m\dot{x}}$, $a_{44} = -\dot{x} + \dfrac{2\left(C_{lf}l_f + C_{cf}l_r\right)}{m\dot{x}}$

$a_{51} = cos\varphi$, $a_{52} = -sin\varphi$, $a_{53} = -\dot{x}sin\varphi - \dot{y}cos\varphi$

$a_{61} = sin\varphi$, $a_{62} = cos\varphi$, $a_{63} = \dot{x}cos\varphi - \dot{y}sin\varphi$

Distracted driver model

Combined with the driver's distracted operating characteristics on long curves, the driver model parameters (preview time t_p, driver neural reaction time t_d, driver operation lag time t_h, steady-state gain coefficient G_{ay}) are adjusted.

Using the driver model from Kong et al.[26], consider the steering behavior of the driver, while incorporating correction and delay components to simulate the delayed reaction characteristics of a distracted driver:

$$\delta_l = \left[\delta_f - \dfrac{I_z\eta}{l_aC_{lf}}(\varphi_r - \varphi_d)\right]\dfrac{exp(-t_ds)}{1+t_hs}\dfrac{1+t_cs}{G_{ay}} \tag{10}$$

Among them:

$$\delta_f = \dfrac{I_z}{l_aC_f}\left[\dfrac{l_a^2C_{lf} + l_b^2C_{cr}}{I_zV_x}\varphi + \dfrac{l_aC_{lf} - l_bC_{cr}}{I_z}\beta - \dot{\varphi}_r\right]$$

$$\varphi_d = 2\left[arctan\left(\dfrac{\Delta f}{V_xt_p}\right) - \beta\right]t_p^{-1}$$

where, V_x represents the longitudinal velocity of the vehicle. β denotes the sideslip angle at the center of mass. δ_f indicates the front wheel steering angle controlled by the sliding mode. φ_d is the desired yaw rate. φ_r is the actual yaw rate. t_p is the preview time, preview time refers to the time that the driver can observe and judge the road conditions ahead in advance during driving. Δf represents the lateral deviation between the preview point and the reference path. η is the coefficient of the reaching law, where $\eta > 0$. $\dfrac{1+t_cs}{G_{ay}}$ is the compensating element,

with G_{ay} being the steady-state gain coefficient of the lateral acceleration. $\dfrac{\exp(-t_d s)}{1 + t_h s}$ represents the response delay element, where $\exp(-t_d s)$ simulates the neural response system of the driver, and t_h is the driver's reaction time.

In a distracted state, drivers not only exhibit delayed reactions but also demonstrate uncertainty in their steering operations. It is therefore imperative to incorporate these uncertain factors into the model of a distracted driver. The steering angle can be represented as:

$$\delta = \theta \delta_l + \Delta \delta_l \qquad (11)$$

In the formula, δ represents the actual steering angle. θ is an uncertainty coefficient that represents the uncertainty of driver modeling. δ_l is the standard steering angle of the sliding mode controller. $\Delta \delta_l$ represents the additional uncertainty in the steering angle due to driver distraction. The final driver model is:

$$\delta = \theta \left[\delta_f - \frac{I_z \eta}{l_a C_{lf}} (\varphi_r - \varphi_d) \right] \frac{exp(-t_d s)}{1 + t_h s} \frac{1 + t_c s}{G_{ay}} + \Delta \delta_l \qquad (12)$$

For distracted drivers, as the preview time decreases and the reaction time increases, their ability to control the vehicle diminishes. Vehicle yaw is the most easily recognized signal by a distracted driver, hence the lateral deviation of the vehicle is used as a quantifiable measure of the distracted driver's steering behavior. The study by Hua et al.[27] analyzes the steering behavior, psychological comfort, and lateral deviation data under cognitive and visual distractions across various curve radii. It notes that under cognitive distraction, drivers exhibited a lateral deviation of 0.345 m on a 200-m radius path. To simulate distracted driving behavior, a simulation was conducted considering the characteristics of distracted drivers, with a set speed of 60 km/h.

By adjusting the driver parameters (preview time t_p, neural reaction time t_d, and operation delay time t_h), the driving performance declines. Cognitive distraction reduces the vehicle's lateral stability and the driver's time to focus on the road ahead. Attentive drivers can anticipate curves and take measures to navigate smoothly, whereas distracted drivers, due to a lack of focus, often miss the optimal moment to anticipate curves, resulting in greater lateral deviation. This deviation not only diminishes driving safety but also indicates an overall decline in driving performance, including extended response times to road conditions and reduced decision-making accuracy. Figure 2 records the changes in steering angle and vehicle lateral deviation of 12 distracted driving experiments, with the average lateral deviation of the 12 experiments being 0.351 m.

Shared control system design incorporating driver behavior

In this section, we design a multi-constraint model predictive controller (H-ORPF-MPC) that incorporates both driver behavior and road environment factors to strengthen collaboration between the driver and the control system. Additionally, a fuzzy controller is introduced to adaptively adjust driving authority based on real-time road safety conditions and driver distraction levels. The proposed shared control framework is depicted in Fig. 3. The shared control system framework is mainly divided into three parts: the human-vehicle control system, the authority allocation module, and the Carsim driving environment module. The vehicle control system integrates the driver model and H-ORPF-MPC, both of which receive vehicle status data. The driver model outputs the driver control angle to H-ORPF-MPC. The core of H-ORPF-MPC includes the vehicle
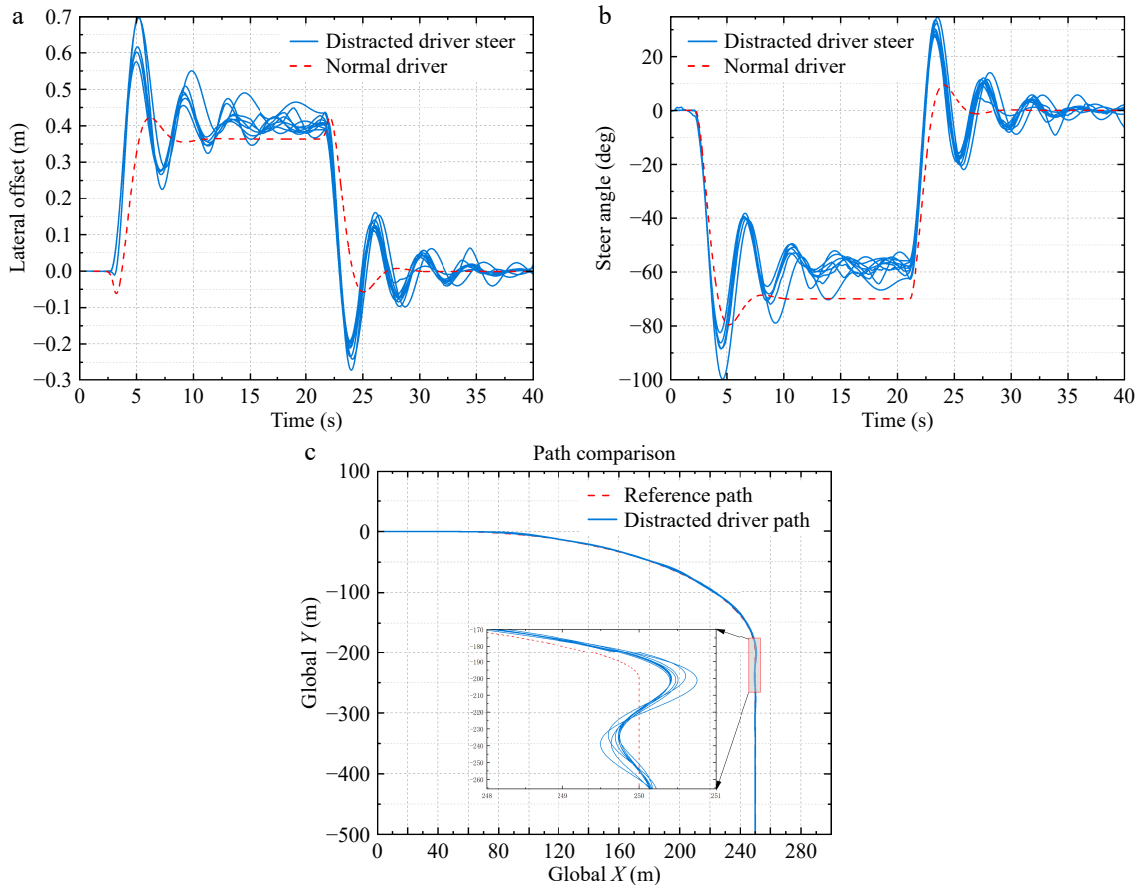
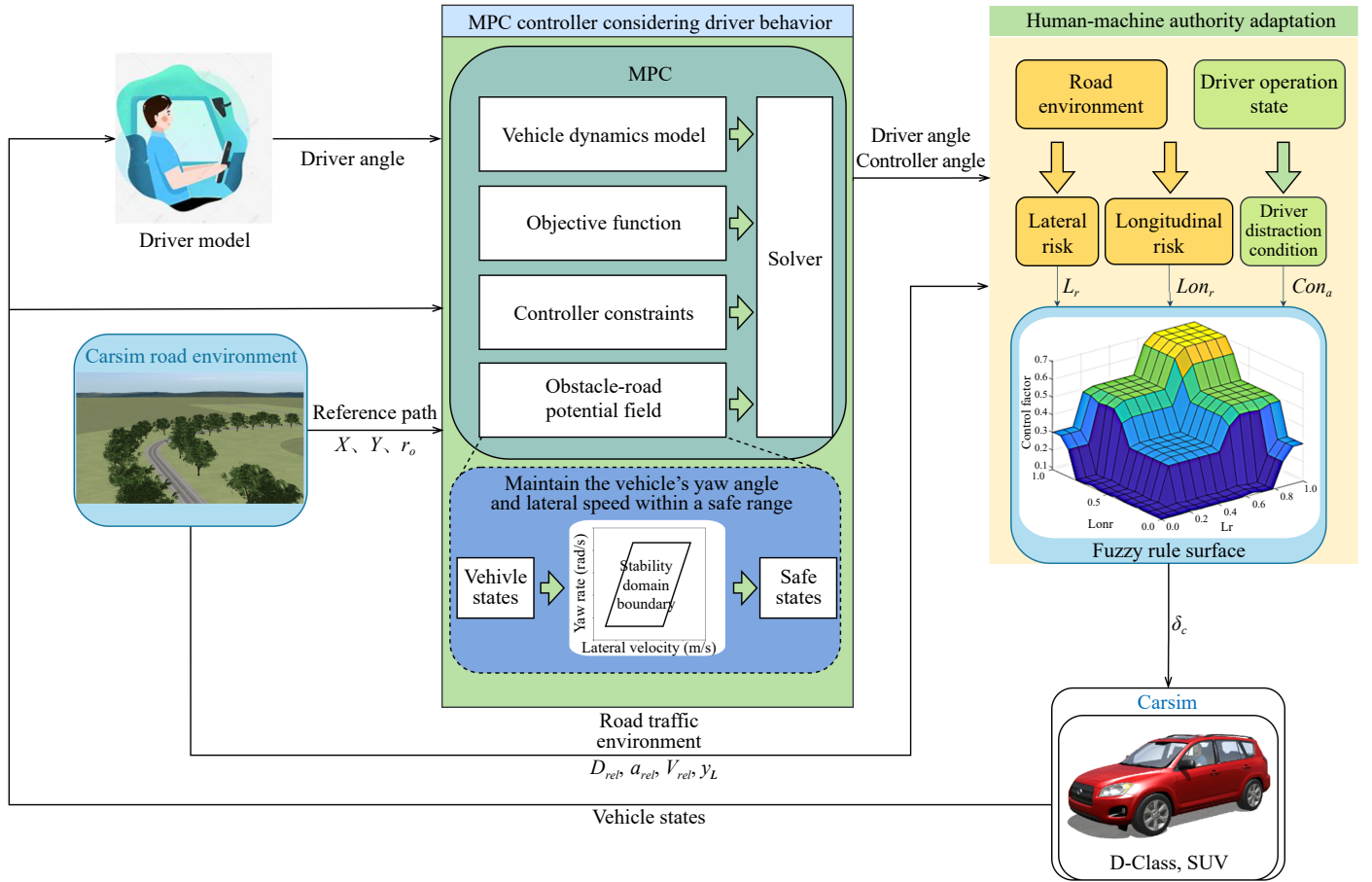**Fig. 2** Driving performance of distracted drivers.

Fig. 3 The framework of a proposed shared control system.

dynamics model, objective function, obstacle-road potential field, and controller constraint settings. The obstacle-road potential field quantifies the risk of obstacles and road boundaries around the host vehicle. The controller constraint part limits the vehicle's state within a safe envelope by limiting the vehicle's lateral speed and yaw angular velocity. H-ORPF-MPC finally outputs the driver's control angle and the controller's angle to the authority allocation module. The authority allocation module will quantify the road environment conditions and driver operating status according to the three set functions. The normalized driver distraction value and road environment risk value are used as the input of the fuzzy controller, and the control authority of the driver controller is determined according to the set fuzzy rules to obtain the final vehicle angle input.

Controller design considering driver behavior and driving environment

In the design of the controller, the driver control action and road environment evaluation function are embedded into the model prediction controller, so that the controller can obtain the optimal solution according to the driver's operation, and the mutual assistance ability of the shared controller and the driver is enhanced. Research indicates that both the lateral velocity and yaw rate of the vehicle are significantly higher under distracted driving conditions compared to normal driving[28]. To address this, a yaw rate-lateral velocity safety envelope is designed as a constraint for the controller.

By incorporating driver control actions, Eqn (9) can be revised as follows:

$$\dot{\chi} = A(t)\chi(t) + B_m(t)U_m(t) + B_h(t)U_h(t) \qquad (13)$$

where,

$$B_m(t) = \begin{bmatrix} \dfrac{2C_{cf}\lambda_{LLC}}{m_2}\left(2\delta_f - \dfrac{\dot{y}+l_f\dot{\varphi}}{s}\right) \\ \dfrac{2\left(C_{lf}s_f - C_{cf}\right)}{m}\lambda_{LLC} \\ 0 \\ \dfrac{2l_f\left(C_{lf}s_f - C_{cf}\right)}{l_z}\lambda_{LLC} \\ 0 \\ 0 \end{bmatrix},$$

$$B_h(t) = \begin{bmatrix} \dfrac{2C_{cf}(1-\lambda_{LLC})}{m_2}\left(2\delta_f - \dfrac{\dot{y}+l_f\dot{\varphi}}{s}\right) \\ \dfrac{2\left(C_{lf}s_f - C_{cf}\right)}{m}(1-\lambda_{LLC}) \\ 0 \\ \dfrac{2l_f\left(C_{lf}s_f - C_{cf}\right)}{l_z}(1-\lambda_{LLC}) \\ 0 \\ 0 \end{bmatrix}$$

The forward Euler discretization method is used to obtain the discrete state space equation:

$$\chi(k+1) = \overline{A}(k)\chi(k) + \overline{B}_m(k)U_m(k) + \overline{B}_h(k)U_h(k)$$

In the above equation, λ_{LLC} is the control collaborative factor, which is determined by the authority allocation strategy between human and machine designed in the next section. The other parameters are vehicle performance parameters. $\overline{A}(k) = I + TA(t)$;

$\overline{B}_m(k) = TB_m(t)$; $\overline{B}_h(k) = TB_h(t)$, where T is the sampling period. This study has systematically derived the state space equations for Model Predictive Control (MPC). Now, the focus is on deriving the cost function and constraints of the controller. To achieve the optimal integration of driving intent with the control system, it is necessary to parameterize and integrate the driver's behavioral preferences into the MPC objective function framework. The mathematical representation of this driving intent can be expressed as:

$$E_{driver} = \frac{|\delta_h - \delta_m|}{H} \tag{14}$$

where, δ_h is the current output action by the driver, δ_m is the optimal solution calculated by the controller at the previous moment and used as the controller's output action, and H is the adjustment coefficient.

In order to evaluate the safety situation around the vehicle when the host vehicle is driving, the artificial potential field[29−31] method is used to construct the obstacle-road potential field (ORPF) to quantify the risks of surrounding obstacles and road boundaries to the host vehicle. Obstacles include roadblocks, pedestrians, vehicles, etc. All objects that may threaten the host vehicle. The obstacle potential field function is as follows:

$$U_{oPF,i}(X,Y) = \frac{\kappa_{oPF,i}}{\left\|\frac{X}{x_i}, \frac{Y}{y_i}\right\|^{b_{oPF,i}}} \tag{15}$$

where, $k_{oPF,i}$ and $b_{oPF,i}$ are both constant, which are expressed as the potential field strength coefficient and shape coefficient of the obstacle, respectively. x_i and y_i represent the relative distance between the main car and the obstacle, respectively. Their specific settings are as follows：

$$x_i = x_0 + v_x T_0 + \frac{\Delta v_{xi}^2}{2a_n}$$
$$y_i = y_0 + (v_x sin\varphi + v_{obsi} sin\varphi)T_0 + \frac{\Delta v_{yi}^2}{2a_n} \tag{16}$$

where, x_0 and y_0 are the minimum safety distances in the horizontal and vertical directions respectively, T_0 is the safety reaction and braking time, v_{obsi} is the speed of the obstacle, Δv_{xi} and Δy_{xi} are the distance between the vehicle and the obstacle The relative speed between them, a_n is the safe acceleration.

The safety risk increases when the vehicle is closer to the lane boundary, so the road boundary material potential field should be inversely proportional to the relative distance between the main vehicle and the road boundary:

$$U_{RPF}(X,Y) = \frac{\kappa_R}{\|X - x_R, Y - y_R\|^2} \tag{17}$$

Among them, k_R is the electric field intensity coefficient of the road, x_R and y_R are the horizontal and vertical coordinates of the lane boundary line. The final defined ORPF function is:

$$U_{ORPF} = \sum_i U_{oPF,i} + \sum_j U_{RPF} \tag{18}$$

Considering the driver's operating intention and the vehicle driving environment, the objective function of MPC is set as follows:

$$J = Q\sum_{i=0}^{N_p-1}\left(\eta(t+i|t) - \eta_{ref}(t+i|t) + E_d\right)^2 +$$
$$R\sum_{i=0}^{N_p-1}(\Delta U_m(t+i|t))^2 + \sum_{i=0}^{N_p-1}U_{ORPF}(t+i|t) + \rho\epsilon^2 \tag{19}$$

Due to the delayed and often unreasonable steering inputs by the driver while driving in a distracted state, significant path-tracking deviations can occur. When the driver recovers from distraction, they must promptly adjust the vehicle's steering angle to return to the desired path, resulting in notable increases in the vehicle's yaw rate and lateral velocity. Considering that visual distraction reduces the vehicle's lateral stability, an envelope constraint is set in the

controller to maintain vehicle safety and prevent loss of stability due to skidding[32].

By setting the rear wheel slip angle constraint as $\alpha_{r,min} \le \alpha_r \le \alpha_{r,max}$ and combining Eqns (1)–(4), the constraint on yaw rate is derived, corresponding to regions 2 and 4 in Fig. 4:

$$\dot{\varphi}_{lim,max} = \left(\frac{\overline{C}_{ar}\alpha_{r,max}(1 + l_a/l_b)}{m\dot{x}}\right) \tag{20}$$

Combining Eqn (5) yields the constraint on lateral velocity, corresponding to the boundaries 1 and 3 in Fig. 4:

$$\alpha_{r,min} \le \frac{\dot{y} - l_a\dot{\varphi}}{\dot{x}} \le \alpha_{r,max} \tag{21}$$

Writing Eqns (20) and (21) in matrix form:

$$D_{lim} = \begin{bmatrix} \alpha_{r,max} & 0 & 0 & l_a & 0 & 0 \\ 0 & 0 & 0 & 1 & 0 & 0 \end{bmatrix} s_{lim} = \begin{bmatrix} v_{y,max} \\ \dot{\varphi}_{lim,max} \end{bmatrix} \tag{22}$$

Further expressed as:

$$-s_{lim} \le D_{lim(t)}X_{(t)} \le s_{lim} \tag{23}$$

Simultaneously, constraints are imposed on the control inputs and control increments:

$$U_{m,min} \le U_m \le U_{m,max}\Delta U_{m,min} \le \Delta U_m \le \Delta U_{m,max} \tag{24}$$

The final controller constraints are:

$$\begin{cases} U_{m,min} \le U_m \le U_{m,max} \\ \Delta U_{m,min} \le \Delta U_m \le \Delta U_{m,max} \\ |D_{lim(t)}X_{(t)}| \le s_{lim} \end{cases} \tag{25}$$

Converting these equations into matrix form for the controller inputs[10,25,33]:

$$\begin{bmatrix} \delta_{f,min} \\ \delta_{f,min} \\ \vdots \\ \delta_{f,min} \end{bmatrix} \le \begin{bmatrix} u_m(k) \\ u_m(k+1) \\ \vdots \\ u_m(k+N_p-1) \end{bmatrix} \le \begin{bmatrix} \delta_{f,man} \\ \delta_{f,man} \\ \vdots \\ \delta_{f,man} \end{bmatrix}$$

$$\begin{bmatrix} \Delta\delta_{f,min} \\ \Delta\delta_{f,min} \\ \vdots \\ \Delta\delta_{f,min} \end{bmatrix} \le \begin{bmatrix} \Delta u_m(k) \\ \Delta u_m(k+1) \\ \vdots \\ \Delta u_m(k+N_p-1) \end{bmatrix} \le \begin{bmatrix} \Delta\delta_{f,min} \\ \Delta\delta_{f,min} \\ \vdots \\ \Delta\delta_{f,min} \end{bmatrix}$$

thus:

$$\begin{bmatrix} I \\ -I \end{bmatrix} U_m(k) \le U_{m,max}$$

$$\begin{bmatrix} I \\ -I \end{bmatrix} \Delta U_m(k) \le \Delta U_{m,max}$$

Similarly, the envelope constraint matrix can be transformed into:

$$-S_{lim} \le \overline{P}\chi + \overline{T}_m U_m + \overline{V}_h U_h \le S_{lim} \tag{26}$$

where,
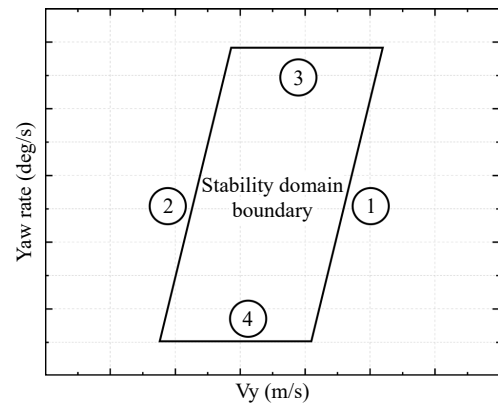
Fig. 4 Stable envelope constraints.

$$\overline{P} = \begin{bmatrix} D_{\lim}\overline{A} \\ D_{\lim}\overline{A}^2 \\ D_{\lim}\overline{A}^3 \\ \vdots \\ D_{\lim}\overline{A}^{N_p} \end{bmatrix}_{6\times N_p\times 6} \quad \overline{V}_\delta = \begin{bmatrix} D_{\lim}\overline{B}_h \\ D_{\lim}(\overline{A}\,\overline{B}_h + \overline{B}_h) \\ D_{\lim}(\overline{A}^2\overline{B}_h + \overline{A}^2\overline{B}_h + \overline{B}_h) \\ \vdots \\ \sum_{k=0}^{N_p-1} D_{\lim}(\overline{A}^k\overline{B}_h) \end{bmatrix}_{6\times N_p\times 1}$$

$$\overline{T}_m = \begin{bmatrix} D_{lim}\overline{B}_m & 0 & \cdots & \cdots & \cdots & 0 \\ D_{lim}\overline{A}\,\overline{B}_m & D_{lim}\overline{B}_m & 0 & \cdots & \cdots & 0 \\ D_{lim}\overline{A}^2\overline{B}_m & D_{lim}\overline{A}\,\overline{B}_m & D_{lim}\overline{B}_m & 0 & \cdots & 0 \\ \vdots & \ddots & \ddots & \ddots & \ddots & \vdots \\ D_{lim}\overline{A}^{N_p-2}\overline{B}_m & \cdots & & D_{lim}\overline{A}\,\overline{B}_m & D_{lim}\overline{B}_m & 0 \\ D_{lim}\overline{A}^{N_p-1}\overline{B}_m & \cdots & & \cdots & D_{lim}\overline{A}\,\overline{B}_m & D_{lim}\overline{B}_m \end{bmatrix}_{6\times N_p\times N_P}$$

Here, u_h represents the driver's input at each sampling instant, and U_m represents the controller's input within the prediction horizon, expressed specifically as:

$$U_m = \begin{bmatrix} u_h(k)\,u_h(k+1)\,u_h(k+2)\cdots u_h(k+N_p-1) \end{bmatrix} \quad (27)$$

The final constraint matrix for the controller is:

$$\begin{bmatrix} \overline{T}_m \\ \overline{T}_m \\ I \\ -I \\ I \\ -I \end{bmatrix} U_m(k) \le \begin{bmatrix} S_{lim} - \overline{P}\chi - \overline{V}_h U_h \\ S_{lim} - \overline{P}\chi - \overline{V}_h U_h \\ U_{m,max} \\ U_{m,max} \\ \Delta U_{m,max} \\ \Delta U_{m,max} \end{bmatrix} \quad (28)$$

Human-machine authority allocation based on fuzzy control

How to allocate steering authority and how the auxiliary system should apply control inputs are key issues in human-machine cooperative control. This section proposes a dynamic steering control authority allocation method based on fuzzy control, considering road environment and driver behavior. The road environment is comprehensively evaluated using the vehicle's lateral risk (L_r) and longitudinal risk (Lon_r), while the driver's distraction level (Con_a) is assessed based on the difference between the driver's control input and the controller's output. The normalized values of these three variables are used as inputs to the fuzzy controller, which outputs a control cooperation factor.

The vehicle's steering action at this point is:

$$\delta_a = \lambda_{LLC}\delta_m + (1 - \lambda_{LLC})\delta_h \quad (29)$$

where, δ_h is the driver's control input, δ_m is the controller's input, λ_{LLC} is the control cooperation factor considering the road driving environment and the driver's steering action, and δ_a is the final vehicle control amount resulting from the combined efforts of the driver and the controller.

The road environment assessment is performed using real-time data on lateral and longitudinal risks. This data, which includes the speed and relative position of surrounding vehicles, is collected using advanced sensors and algorithms. Driving risk is evaluated using Time-to-Collision (TTC) for longitudinal risk and the vehicle's lateral offset for lateral risk.

The lateral risk is measured by the vehicle's lateral offset and quantified using the road width information. The lateral risk coefficient increases in stages with the lateral offset. When the vehicle's offset is within 0.1 meters, it is considered safe. Between 0.1 and 0.3 m, the lateral risk increases with the offset. When the offset reaches 0.3 to 0.45 m, the lateral risk remains at 0.5. However, if the offset continues to increase beyond 0.45 m, the lateral risk increases further until it reaches 1.0 at an offset of 0.7 m, indicating the vehicle is at the road edge and at maximum lateral risk. The lateral risk formula is set as follows:

$$L_r = \begin{cases} 0 & 0.1 > y_L \ge 0 \\ -0.25 + 2.5y_L & 0.3 > y_L \ge 0.1 \\ 0.5 & 0.45 > y_L \ge 0.3 \\ -0.4 + 2y_L & 0.7 > y_L \ge 0.45 \\ 1 & y_L \ge 0.7 \end{cases} \quad (30)$$

Time-to-Collision (TTC) is widely used in driving risk assessment. To make longitudinal risk increase with decreasing TTC, the inverse of TTC (TTCi) is used as the longitudinal risk indicator. TTCi intuitively represents the interaction between the vehicle and its surroundings, especially the relative motion and potential collision risk with the vehicle ahead. A higher TTCi indicates a shorter time to collision and thus a higher longitudinal risk. The formula for TTCi is as follows:

$$TTCi = \begin{cases} \dfrac{v_{rel}}{D_{rel} - d_0} & a_{rel} = 0 \\ \dfrac{a_{rel}}{-v_{rel} + \sqrt{v_{rel}^2 + 2a_{rel}(D_{rel} - d_0)}} & a_{rel} \ne 0 \end{cases} \quad (31)$$

where, D_{rel} is the relative distance between two vehicles, d_0 is the safe stopping distance, and v_{rel} is the relative speed between the two vehicles. TTC is a dynamic metric that can be influenced by many factors, including vehicle speed, road conditions, and driver reaction time. Many studies in the field of vehicle safety have set standards or recommended values for TTC based on different driving environments. It is generally considered safe when the TTC value is above 2 s, high risk when below 2 s, a warning may be issued when in the range of 1.5 to 2 s to remind the driver to take action, and collision is deemed imminent when TTC is below 1 s requiring immediate avoidance measures[34–37]. Considering the curved road setting in this study, the TTC is set to 2.6 s to allow the driver to maintain autonomous control within a safe distance without unnecessary interference. In the range of 1.6 to 2.6 s, potential hazards need to be addressed with preventive measures instead of suddenly increasing the controller authority which could cause anxiety. When TTC is less than or equal to 0.6 s, the system should take immediate action to minimize collision consequences to the greatest extent. This setting ensures rapid response in emergencies to protect driver and passenger safety.

The equation for setting Lon_r is as follows:

$$Lon_r = \begin{cases} 0 & TTCi \le \dfrac{1}{2.6} \\ \left(TTCi - \dfrac{1}{2.6}\right) \times \dfrac{0.5}{\left(\dfrac{1}{10} - \dfrac{1}{20}\right)} & \dfrac{1}{2.6} < TTCi \le \dfrac{1}{1.6} \\ 0.5 + \left(TTCi - \dfrac{1}{1.6}\right) \times \dfrac{0.5}{\left(\dfrac{1}{0.6} - \dfrac{1}{1.6}\right)} & \dfrac{1}{1.6} < TTCi \le \dfrac{1}{0.6} \\ 1 & TTCi > \dfrac{1}{0.6} \end{cases} \quad (32)$$

The driver's distraction is evaluated based on the deviation of the driver's output from the controller's output, which increases with the duration of distraction. This deviation is represented by the difference between the driver's output angle and the desired angle. The distraction level function (Con_a) is designed as follows:

$$Con_a = \begin{cases} 0, & |\delta_h - \delta_m| = 0 \\ \dfrac{|\delta_h - \delta_m|}{|\delta_h - \delta_m|_{max}}, & 0 < |\delta_h - \delta_m| < |\delta_h - \delta_m|_{max} \\ 1, & |\delta_h - \delta_m| > |\delta_h - \delta_m|_{max} \end{cases} \quad (33)$$

The normalized driver distraction and driving risk values are used as inputs to the fuzzy controller. The fuzzy subsets for L_r, Lon_r and Con_a are [S, MS, M, MD, D], representing small, moderately small, medium, moderately large, and large states, respectively. The input variables use triangular membership functions. The output variable

is the cooperation factor, with fuzzy subsets [S, MS, M, MD] representing small, moderately small, medium, and moderately large states. The normalized driver distraction and driving risk values are used as inputs to the fuzzy controller. The fuzzy subsets for L_r, Lon_r, and Con_a are [S, MS, M, MD, D], representing small, moderately small, medium, moderately large, and large states, respectively. The input variables use triangular membership functions. The output variable is the cooperation factor, with fuzzy subsets [S, MS, M, MD] representing small, moderately small, medium, and moderately large states. The principle for adjusting the collaborative control factors is as follows: To ensure driver comfort, the fuzzy rules are primarily based on the driver's state while also considering vehicle safety. When the driver is not distracted, no auxiliary control is needed, and the cooperation factor is zero. When the driver is slightly distracted, the auxiliary control effort is determined by the vehicle's lateral and longitudinal risks, with a preference towards driver comfort. If either risk is low, the cooperation factor is small; if either risk is high, indicating deteriorating vehicle safety, the cooperation factor is large. When both risks are high, indicating the vehicle is on the verge of losing control, the cooperation factor is maximized for immediate correction by the auxiliary controller. When the driver is moderately distracted, the cooperation factor is determined equally by the driver and the auxiliary controller. When the driver is severely distracted, the auxiliary controller's authority is prioritized to maintain vehicle safety. The fuzzy rules for the cooperation factor are shown in Table 1, and the corresponding fuzzy rule surface diagram is shown in Fig. 5.

Simulation and discussion

In this section, the designed controller and human-machine authority allocation strategy are verified through simulations conducted on the Simulink and CarSim platforms. In Simulink, a distracted driver model, a vehicle-road model, an MPC module

considering driver behavior output constraints, and a human-machine authority allocation module is established. In CarSim, an SUV model is selected, and the road model consists of a 50 m straight path, a 200 m radius curve, and a 100 m three-section path. The road has two lanes, each 3.75 m wide, with a friction coefficient of $\mu = 0.85$. A leading vehicle is set to move at 13 m/s in another lane, 50 m ahead of the test vehicle, which overtakes it after 12 s. The parameters used in the experiment are shown in Table 2.

Figure 6a shows the steering angle performance of the driver and the controller before and after adding fuzzy control. Without the fuzzy controller, the driver's steering operation exhibits significant overshoot and subsequent oscillation due to reaction delay during cornering. Although the designed MPC considering driver behavior maintains a smaller steering angle, it still shows slight oscillation due to the driver's steering input. After adding the fuzzy controller, the driver's steering angle reduces without overshoot and oscillation, and the controller's steering input becomes more stable, eliminating oscillation. This indicates that the designed controller can mitigate the delayed steering actions of the driver, making the steering operation more stable and safer. To further verify the performance of the proposed controller, human-machine conflict evaluation index J_{c1} and driving comfort evaluation index J_{c2}[12,19] are introduced to compare the changes of each index before and after adding the proposed controller for each sampling period. The current corner steering trend is represented by the corner slope,
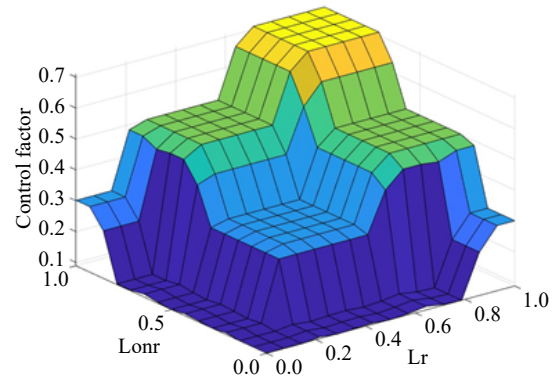
Fig. 5 Fuzzy surfaces of fuzzy rules.

Table 1. Fuzzy rules.

Con_a	Lon_r	L_r				
		S	MS	M	MD	D
S	S	S	S	S	S	S
	MS	S	S	S	S	S
	M	S	S	S	S	S
	MD	S	S	S	S	MS
	D	S	S	S	MS	MS
MS	S	S	S	S	MS	MS
	MS	S	S	S	MS	MS
	M	S	S	MS	MS	M
	MD	S	S	MS	M	M
	D	S	MS	MS	M	MD
M	S	S	S	S	S	MS
	MS	S	MS	MS	M	M
	M	S	MS	MS	M	M
	MD	S	M	M	MD	MD
	D	MS	M	M	MD	MD
MD	S	S	S	MS	M	M
	MS	S	MS	M	M	M
	M	MS	M	M	M	M
	MD	MS	M	M	MD	M
	D	M	M	M	MD	MD
D	S	MS	MS	MS	M	M
	MS	MS	MS	M	M	M
	M	MS	M	M	M	M
	MD	MS	M	M	MD	MD
	D	MS	M	M	MD	MD

Table 2. Parameters in the experiment.

Notation	Meaning	Value
m	Vehicle mass	1,624 (kg)
I_z	Yaw moment of inertia	2,059.2 (kg·m^2)
a	Distance to front axle	1.05 (m)
b	Distance to rear axle	1.61 (m)
S_f	Front slip ratio	0.2
S_r	Rear slip ratio	0.2
C_{cf}/C_{lf}	Front cornering stiffness ratio	66,900 (N/rad)
C_{cr}/C_{lr}	Rear cornering stiffness ratio	62,700 (N/rad)
y_L	Preview distance	14.5 (m)
t_p	Driver preview time	0.9 (s)
t_h	Driver reaction time	0.6 (s)
t_d	Neural time delay	0.3 (s)
V_y	Longitudinal velocity	60 (km/s)
T	Sampling time	0.025 (s)
N_p	Prediction horizon	30
Q	Output weighting matrix	diag (250, 200, 100, 10)
R	Control weight	100
H	Driver weight	2

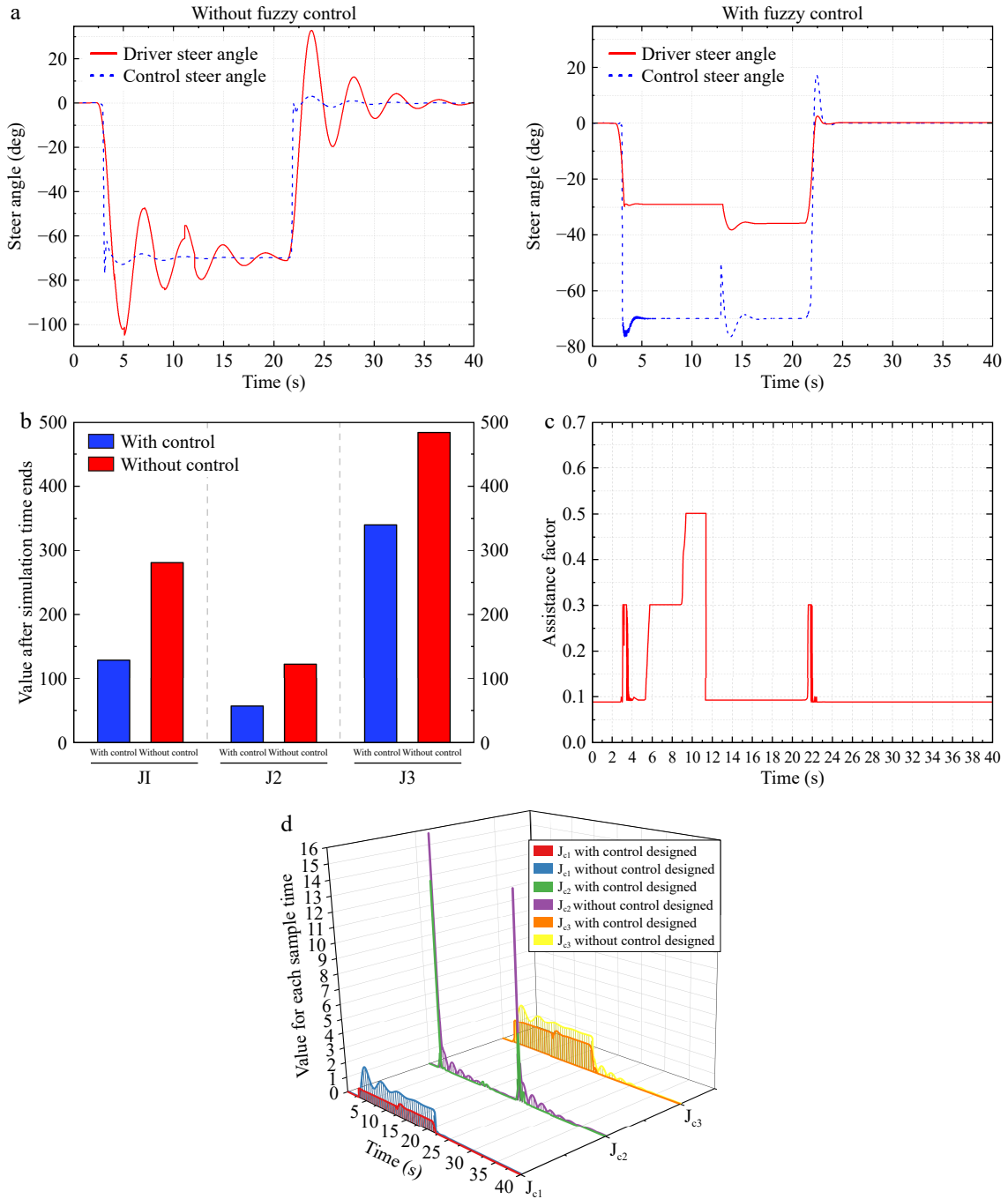Adaptive shared control for distracted drivers

Fig. 6 Experimental results of the curved road scenario.

and the difference in corner slope between the driver and the controller is calculated J_{c1}. When the steering angle slopes of the driver and the controller are similar, it means that the steering intentions of the two are consistent, and the human-machine conflict is considered to be minimal; when the signs of the steering angle slopes of the two are opposite, it means that the steering intentions of the driver and the controller are in conflict, and the human-machine conflict is considered to be the largest. The speed of vehicle steering angle change directly affects the overall comfort of the vehicle, so the absolute value and calculation J_{c2} of the driver's and controller's steering angle rates are set. The smaller the corner speed is, the smoother the vehicle is driving and the better the comfort. The angle difference between the driver and the controller best reflects the output difference between the two. When the

difference is larger, the shared controller output has a greater impact on the final result, and the final output angle deviates further from the driver's angle. Therefore, the intervention degree evaluation index J_{c3} is set to visually display the intervention of the shared controller on the driver. As shown below:

$$J_{c1} = \int_{t}^{t+T} |\dot{\delta}_h - \dot{\delta}_m| dt$$

$$J_{c2} = \int_{t}^{t+T} |\dot{\delta}_m| + |\dot{\delta}_h| dt$$

$$J_{c3} = \frac{\int_{t}^{t+T} |\delta_h - \delta_m| dt}{T} \quad (34)$$

As shown in Fig. 6b, the addition of the proposed shared controller reduced the human-machine conflict by 54%. This indicates that the proposed strategy for switching control authority

between man and machine can mitigate the problem of generating more conflicts with the steering assist system due to excessive steering actions by the driver. At the same time, since the controller can correct inappropriate steering operations, the driving comfort for the driver has been improved by 50% as the lateral behavior is stabilized. Since the driver's operating intention is taken into account when setting the controller and the driving authority allocation strategy, the intervention of the shared controller on the driver is reduced, and the degree of intervention of the shared controller on the driver is reduced by 42%. Figure 6d shows the changes in the three evaluation indicators in each sampling period in detail. It is worth noting that at 12 s, because the vehicle must maintain an appropriate safe distance from the approaching vehicle when overtaking, the steering assistance system increases the control authority of the shared controller. The index J_{c2} is higher than the steering assistance system without a fuzzy controller in a short period of time.

Figure 6c depicts the variation of the cooperation factor. At around 3 s, during corner entry, the significant difference between the driver's steering input and the controller's steering input, along with the substantial lateral offset, results in a cooperation factor of 0.3, although the collision risk is relatively low. By 3.5 s, the lateral deviation has decreased to a small level, and the cooperation factor is reduced to its minimum. To ensure that the controller remains active in the control loop, the cooperation factor cannot be 0. Between 5.3 and 8.9 s, the collision risk begins to increase to a relatively dangerous level, and the cooperation factor is kept at 0.3. Subsequently, from 8.9 to 11.3 s, the collision risk reaches its peak, prompting the cooperation factor to adjust to 0.5 to steer the vehicle away from the adjacent car. Afterward, the vehicle's state

stabilizes, and the cooperation factor is reduced to its minimum. At 22 s, while exiting the curve, the difference between the driver's steering input and the controller's steering angle increases, along with a rise in lateral deviation. Consequently, the cooperation factor is raised back to 0.3. The lateral offset scenario is illustrated in Fig. 7a.

Figure 7a shows the vehicle's trajectory y with and without the controller's assistance. It is evident that with a distracted driver alone, the vehicle significantly deviates from the target trajectory during cornering and experiences overshoot when exiting the curve. With the designed shared controller, the vehicle can consistently track the reference trajectory.

Figure 7b demonstrates the vehicle's trajectory before and after the addition of the controller. The driver exhibits significant deviations during both corner entry and exit, and due to delayed reactions, oscillations occur around 10 s. The maximum lateral deviation reaches 0.7 m at 5 s into the curve and −0.27 m at 22 s when exiting the curve. With the controller, the maximum lateral deviation reduces to 0.023 m at 3.7 s into the curve and 0.0125 m at 21.9 s. At 12 s, since the main vehicle has to overtake the vehicle in the adjacent lane, the lateral risk increases, and the controller assists the driver to correct the deviation in advance to prevent it from getting too close to other vehicles. The results indicate that the designed controller improves vehicle tracking accuracy and reduces collision risk.

Figure 7c shows that at around 3 s, the driver's yaw rate fluctuates during corner entry, peaking at 0.124 rad/s. With the designed controller assisting the distracted driver, the maximum yaw rate during corner entry reduces to 0.095 rad/s. Similarly, the peak yaw rate at the curve exit is 0.037 rad/s without the controller and only
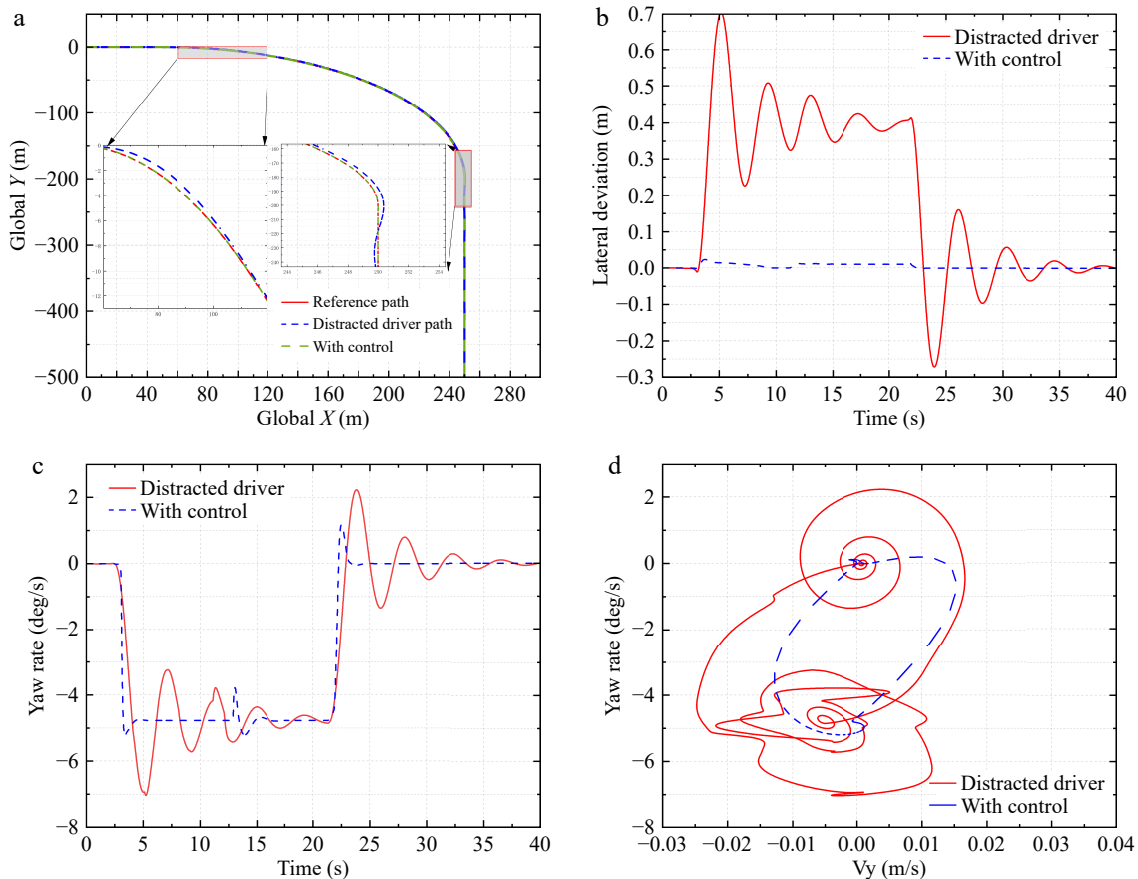

Fig. 7 Experimental results of a curved road scenario.

0.0157 rad/s with the controller. This demonstrates that the designed controller provides better driving stability and comfort. Figure 7d illustrates the lateral stability of the vehicle. The vehicle driven by the distracted driver exhibits significant variations in yaw rate and lateral speed, especially in yaw rate. In contrast, the vehicle with the controller consistently operates within a stable range.

Conclusions

This paper proposes a shared control approach that accounts for the operating characteristics of distracted drivers, facilitating the allocation of driving authority between the driver and the shared controller to enhance driver safety and comfort. To model distracted drivers' steering behavior, this study integrates findings on distracted driving behavior, adjusting driver model parameters to reflect operational uncertainty.

To ensure both safety and comfort, a multi-constraint model predictive controller (H-ORPF-MPC) is developed, which incorporates driver steering actions and utilizes an artificial potential field-based approach. A vehicle state safety envelope is also implemented to maintain control stability. For human-machine authority allocation, lateral offset and Time-to-Collision index (TTCi) serve as road safety risk assessment indicators, while the difference between the driver's output angle and the expected angle is used to gauge driver distraction. These indicators are normalized, fuzzified, and coordinated through a fuzzy control mechanism to achieve an optimal collaboration factor.

Future research will focus on exploring additional methods to represent driver behavior more comprehensively, incorporating dynamic driver status into controller design and driving authority allocation strategies to better adapt to varying driver conditions.

Author contributions

The authors confirm contribution to the paper as follows: conceptualization, methodology, draft manuscript preparation: Liao L, Xing P; software: Xing P; data curation: Xing P; analysis and interpretation of results: Gan Z, Wei X, Liu Y; supervision, project administration, funding acquisition: Liao L. All authors reviewed the results and approved the final version of the manuscript.

Data availability

The datasets generated during and analyzed during the current study are available from the corresponding author on reasonable request.

Acknowledgments

Conflict of interest

The authors declare that they have no conflict of interest. Lyuchao Liao is the Editorial Board member of *Digital Transportation and Safety* who was blinded from reviewing or making decisions on the manuscript. The article was subject to the journal's standard procedures, with peer-review handled independently of this Editorial Board member and the research groups.

References

1. Vosugh N, Bahmani Z, Mohammadian A. 2023. Distracted driving recognition based on functional connectivity analysis between physiological signals and perinasal perspiration index. *Expert Systems with Applications* 231:120707
2. Née M, Contrand B, Orriols L, Gil-Jardiné C, Galéra C, et al. 2019. Road safety and distraction, results from a responsibility case-control study among a sample of road users interviewed at the emergency room. *Accident Analysis & Prevention* 122:19−24
3. Caballero WN, Naveiro R, Ríos Insua D. 2022. Modeling ethical and operational preferences in automated driving systems. *Decision Analysis* 19:21−43
4. Jia X, Tong Y, Qiao H, Li M, Tong J, et al. 2023. Fast and accurate object detector for autonomous driving based on improved YOLOv5. *Scientific Reports* 13:9711
5. Zhai S, Wang L, Liu P. 2023. Human and machine drivers: Sharing control, sharing responsibility. *Accident Analysis & Prevention* 188:107096
6. Mello JE, Hunt CS, Mello AL. 2018. Driver control practices: the voice of the driver. *Transportation journal* 57:53−82
7. Jiang Y, Deng W, Wu J, Zhang S, Jiang H. 2019. Adaptive steering feedback torque design and control for driver–vehicle system considering driver handling properties. *IEEE Transactions on Vehicular Technology* 68:5391−406
8. Wang J, Zheng H, Zong C. 2019. Longitudinal and lateral dynamics control of automatic lane change system. *Transactions of the Institute of Measurement and Control* 41:4322−38
9. Jiang Y, Zhu B, Yang S, Zhao J, Deng W. 2023. Vehicle trajectory prediction considering driver uncertainty and vehicle dynamics based on dynamic bayesian network. *IEEE Transactions on Systems, Man, and Cybernetics: Systems* 53:689−703
10. Chen Y, Zhang X, Wang J. 2021. Robust vehicle driver assistance control for handover scenarios considering driving performances. *IEEE Transactions on Systems, Man, and Cybernetics: Systems* 51:4160−70
11. Chen G, Chen S, Langari R, Li X, Zhang W. 2019. Driver-behavior-based adaptive steering robust nonlinear control of unmanned driving robotic vehicle with modeling uncertainties and disturbance observer. *IEEE Transactions on Vehicular Technology* 68:8183−90
12. Nguyen AT, Sentouh C, Popieul JC. 2017. Driver-automation cooperative approach for shared steering control under multiple system constraints: Design and experiments. *IEEE Transactions on Industrial Electronics* 64:3819−30
13. Sentouh C, Nguyen AT, Benloucif MA, Popieul JC. 2019. Driver-automation cooperation oriented approach for shared control of lane keeping assist systems. *IEEE Transactions on Control Systems Technology* 27:1962−78
14. Chen Y, Hu C, Wang J. 2020. Impaired driver assistance control with gain-scheduling composite nonlinear feedback for vehicle trajectory tracking. *Journal of Dynamic Systems, Measurement, and Control* 142:071003
15. Singh R, Sah CK, Keshavan J. 2024. Adaptive koopman embedding for robust control of complex nonlinear dynamical systems. *arXiv* Preprint
16. Lym Y, Chen Z. 2021. Influence of built environment on the severity of vehicle crashes caused by distracted driving: A multi-state comparison. *Accident Analysis & Prevention* 150:105920
17. Huang C, Naghdy F, Du H, Huang H. 2019. Shared control of highly automated vehicles using steer-by-wire systems. *IEEE/CAA Journal of Automatica Sinica* 6:410−23
18. Flad M, Fröhlich L, Hohmann S. 2017. Cooperative shared control driver assistance systems based on motion primitives and differential games. *IEEE Transactions on Human-Machine Systems* 47:711−22
19. Fang Z, Wang J, Wang Z, Liang J, Liu Y, et al. 2023. A human-machine shared control framework considering time-varying driver characteristics. *IEEE Transactions on Intelligent Vehicles* 8:3826−38

20. Li Y, Sun D, Zhao M, Chen J, Liu Z, et al. 2020. MPC-based switched driving model for human vehicle co-piloting considering human factors. *Transportation research part C: emerging technologies* 115:102612

21. Jiang Y, Ding Y, Zhang X, Xu X, Huang J. 2024. A self-learning human-machine cooperative control method based on driver intention recognition. *CAAI Transactions on Intelligence Technology* 9:1101−115

22. Dong N, Wu Z, Gao Z. 2024. Shared control based on ANFIS for brain-controlled driving. *Transactions of the Institute of Measurement and Control* 46:579−91

23. Zhao X, Yin Z, He Z, Nie L, Li K, et al. 2023. Indirect shared control strategy for human-machine cooperative driving on hazardous curvy roads. *IEEE Transactions on Intelligent Vehicles* 8:2257−70

24. Gong J, Jiang Y, Xu W. 2014. *Model predictive control for self-driving vehicles*. Beijing Institute of Technology Press: Beijing, China. pp. 38−39

25. Lu Y, Liang J, Yin G, Xu L, Wu J, et al. 2023. A shared control design for steering assistance system considering dri ver behaviors. *IEEE Transactions on Intelligent Vehicles* 8:900−11

26. Kong X, Deng Z, Yu S, Yi Q, Jin Y. 2020. Driver model of vehicle lateral preview based on sliding mode control. *Journal of Hubei University of Automotive Technology* 34(4):25−28

27. Hua Q, Jin L, Jiang Y, Guo B, Xie X. 2021. Effect of cognitive distraction on physiological measures and driving performance in traditional and mixed traffic environments. *Journal of Advanced Transportation* 2021:6739071

28. Chen Z, Wu C, Zhong M, Lyu N, Huang Z. 2015. Identification of common features of vehicle motion under drowsy/distracted driving: a case study in Wuhan, China. *Accident Analysis & Prevention* 81:251−59

29. Li M, Cao H, Li G, Zhao S, Song X, et al. 2020. A two-layer potential-field-driven model predictive shared control towards driver-automation cooperation. *IEEE transactions on intelligent transportation systems* 23:4415−31

30. Fan X, Guo Y, Liu H, Wei B, Lyu W. 2020. Improved artificial potential field method applied for AUV path planning. *Mathematical Problems in Engineering* 2020:6523158

31. Sang H, You Y, Sun X, Zhou Y, Liu F. 2021. The hybrid path planning algorithm based on improved A* and artificial potential field for unmanned surface vehicle formations. *Ocean Engineering* 223:108709

32. Shi P, Jiang J, Hou J, Liang M, Zheng L, et al. 2021. Research on path following control off our-wheel steering vehicle considering driving stability. *Journal of Guangxi University (Natural Science Edition)* 46(3):606−14

33. Li R, Li Y, Li SE, Burdet E, Cheng B. 2017. Driver-automation indirect shared control of highly automated vehicles with intention-aware authority transition. *2017 IEEE Intelligent Vehicles Symposium (IV), 11−14 June 2017, Los Angeles, CA, USA*. USA: IEEE. pp. 26−32. doi: 10.1109/IVS.2017.7995694

34. Chen R, Sherony R, Gabler HC. 2016. Comparison of time to collision and enhanced time to collision at brake application during normal driving. *SAE Technical Paper. Rep. 0148-7191*. doi: 10.4271/2016-01-1448

35. Nadimi N, NaserAlavi SS, Asadamraji M. 2022. Calculating dynamic thresholds for critical time to collision as a safety measure. *Proceedings of the Institution of Civil Engineers - Transport* 175:403−12

36. Fu Y, Li C, Yu FR, Luan TH, Zhang Y. 2022. A survey of driving safety with sensing, vehicular communications, and artificial intelligence-based collision avoidance. *IEEE Transactions on Intelligent Transportation Systems* 23:6142−63

37. Orsini F, Gecchele G, Rossi R, Gastaldi M. 2021. A conflict-based approach for real-time road safety analysis: comparative evaluation with crash-based models. *Accident Analysis & Prevention* 161:106382